Acta Crystallographica Section D
Biological Crystallography
ISSN 0907-4449

SAD phasing with triiodide, softer X-rays and some help from radiation damage

Gwyndaf Evans,[a] Maurizio Polentarutti,[b] Kristina Djinovic Carugo[b] and Gérard Bricogne[a]*

[a]Global Phasing Ltd, Cambridge CB3 0AX, England, and [b]Structural Biology Laboratory, Sincrotrone Trieste in Area Science Park, S.S. 14 km 163.5, I-34012 Basovizza (TS), Italy

Correspondence e-mail: gb10@globalphasing.com

Received 7 March 2003
Accepted 5 June 2003

SAD data on a triiodide derivative of porcine pancreatic elastase have been recorded from a single sample using 2.0 Å wavelength X-rays. The large anomalous signal of iodine at this wavelength allowed the detection of heavy-atom sites and subsequent structure determination using low-redundancy data. Substantial radiation damage was observed during the measurements and this prevented the merging together of all data. However, a straightforward treatment of the radiation effects on the heavy-atom model during parameter refinement resulted in additional phase information being gleaned from the observed reduction in iodine occupancy factors, which in turn produced a significant improvement in the quality of the electron-density map.

1. Introduction

In recent years, a number of groups have turned their attention to developing fast heavy-atom derivative preparation methods for use either in-house or at synchrotrons. The aims of these studies have been to provide crystallographers with a greater variety of methods for preparing heavy-atom derivatives and obtaining experimental phase information, and thereby complement the current developments in high-throughput structure determination (Dauter, 2002).

The developments have included short cryosoaking methods with the halides Br^- and I^- (Dauter *et al.*, 2000), the use of positively and negatively charged counter ions Gd^{3+}, Cs^+, I^- and Cl^- (Nagem *et al.*, 2001; Evans & Bricogne, 2002); the use of triiodide, I_3^- (Evans & Bricogne, 2002); Xe derivatization under pressure (see Sauer *et al.*, 1997; Djinovic Carugo *et al.*, 1998; Panjikar & Tucker, 2002*a*, and references therein); combinations of halides and Xe (Panjikar & Tucker, 2002*b*); and short soaks with traditional heavy-atom compounds (Sun *et al.*, 2002; Sun & Radaev, 2002). These studies have been performed in-house with Cu $K\alpha$ radiation or at synchrotron sources with wavelengths <1.6 Å.

The *L* absorption edges of a number of elements which are interesting to macromolecular crystallographers, *e.g.* I, Xe and Cs and some lanthanides, lie between 2.7 and 2.0 Å (4.60 and 6.2 keV). Within this range f'' can reach as much as 14 e and thus by recording data at longer wavelengths there is a possible gain by a factor of two in signal compared with measuring at 1.54 Å. This was indeed observed by Cianci *et al.* (2001) who recorded data from a Xe derivative of lobster apocrustacyanin A_1 at a wavelength of 2.045 Å where $f''(\mathrm{Xe}) = 11.5$ e. Data collection using softer[1] X-rays has been of particular use in phase-determination efforts using native S anomalous signal (Micossi *et al.*, 2002; Dauter, 2002) and is

[1] We have adopted the term 'softer' X-rays proposed by Cianci *et al.* (2001).

indeed well on the way to becoming a routine source of additional anomalous signal (Weiss *et al.*, 2001).

In this paper, we investigate for the first time the combination of the use of short-soak derivatization using triiodide solutions and data collection with softer synchrotron X-rays and attempt to take advantage of the significant anomalous signal offered by the increase in f'' for iodine at these wavelengths..

2. Experimental methods

2.1. Experimental apparatus

Experiments were performed on beamline XRD1 at the Elettra synchrotron source. The beamline uses a MAR Research slit-box and rotation-axis assembly, and a 165 mm MAR-CCD detector. The sample is cooled using a modified Oxford Cryosystems cryostream (K. Djinovic, personal communication) which provides a constant flow of dry He gas at 100 K and simultaneously floods the sample environment which is enclosed and kept at a positive pressure of He (Polentarutti & Djinovic Carugo, 2003). This provides a low-absorption diffracted beam path between sample and detector and reduces the effects of air scatter and air absorption at longer wavelengths.

2.2. Sample preparation

Crystals of porcine pancreatic elastase (PPE) were produced and a triiodide derivative was prepared as described previously (Evans & Bricogne, 2002) by soaking a crystal for 4 min in a solution of 20 m*M* KI/I_2, 1 m*M* Na_2SO_4, 10 m*M* CH_3COONa pH 5.0 and 25% glycerol. The crystal was mounted directly from the cryosoak solution into the 100 K He-gas stream. A test diffraction pattern showed that the crystal diffracted to beyond 1.8 Å.

2.3. Data measurement and analysis

When measuring diffraction from a protein crystal of typical size using long wavelengths, absorption effects can become very significant (Arndt, 1984). Indeed, data must be carefully treated to correct for these effects (Weiss *et al.*, 2001). With this in mind, an effort was made to record diffraction data in such a way that empirical absorption corrections could be well determined. For this purpose, it is beneficial to have measurements of reflections which have passed through and therefore sampled all possible absorption paths through the crystal. Ideally, equivalent Bragg intensities should be recorded multiple times, entering and leaving the sample volume at all points on the absorption surface. In the rotation method, this ideal situation can only be approximated with the use of a multi-axis goniometer whereby the crystal can be reoriented a number of times during the experiment to allow the whole absorption surface of the crystal to be sampled and later modelled by empirical means.

In the absence of a motor-controlled multi-axis goniometer, the crystal was mounted on a twin-arc Huber goniometer head which allowed $\pm 15^\circ$ of motion around axes perpendicular to the horizontal data-collection axis. A careful note was made of the laboratory frame vectors describing the rotations of the two arcs and this information was then given to the data-integration package *d*TREK* (Pflugrath, 1999) along with the arc angle settings ($\pm 0.2^\circ$) read directly from the goniometer head. This ensured that data sets recorded in different orientations could be indexed using a common setting to ensure a proper treatment of absorption.

The *L* edges of iodine are at 2.3898, 2.5553 and 2.7208 Å. Neglecting XANES effects, which appear to produce no significant enhancement of f'' (Konishi *et al.*, 2001), the maximum f'' signal attainable in this energy regime is 13.5 e (Cromer & Liberman, 1970) at the L_I edge. One disadvantage of measuring at long wavelengths is a reduction in data resolution owing to the expansion of the diffraction pattern at the detector surface. The beamline geometry means that with $\lambda = 2.3898$ Å the maximum resolution of data with the detector set at 37 mm would be 2.2 Å. Minimum I–I distances in polyhalides are $\sim$2.7 Å and individual I atoms would probably have been resolvable with 2.22 Å data; however, because of the strong diffraction properties of the sample and the additional benefits of reduced absorption, it was decided to measure data with $\lambda = 2.0$ Å and tolerate a decrease in f'' from 13.5 to 10.4 e. It is beyond the scope of this paper to investigate the relative benefits of increased data resolution over reduced anomalous signal.

The first data set (DS1) was recorded with both arcs set to -15°. In this setting 200° of data were recorded using 0.5° rotation widths and a 4 s exposure time. The arcs were then reset to $+15^\circ$ and a further 200° of data (DS2) were measured from the same sample using the same data-collection parameters. The main consideration in following this protocol was to record data in two settings separated by as large an angle as possible. Initial indexing of the diffraction pattern showed that the b^* axis was almost parallel to the spindle rotation axis in the first orientation. This would result in an absence of some data owing to the blind region, but it was assumed that the second orientation would allow any missing data to be measured.

The integrated reflection data, together with complete goniometric information from *d*TREK*, were converted into a multi-record MTZ file (Collaborative Computational Project, Number 4) using the program *DTREK2SCALA*.[2] Image scale and *B* factors, along with an empirical spherical harmonic absorption correction, were determined and applied using *SCALA* (Evans, 1997).

3. Results

The results from *SCALA* showed clear evidence of radiation damage in the samples and of its steady increase over the course of the experiment. The image *B* factor relative to the first image had increased to over 15 $Å^2$ by the end of the

[2] A derivative of the *CCP*4 program *ABSURD* modified by GE to convert *d*TREK* reflection files and geometric information into MTZ format. To be included in *CCP*4 release 5.0.

Table 1
Results of data analysis illustrating the good individual quality of the two data sets but the poor merging statistics resulting from radiation damage.

The multiplicity-weighted R factor, R_{meas}, doubles when the two data sets are merged together, providing strong evidence that some structural change has occurred in the sample crystal. The low overall completeness of DS1 is because of the 'fortuitous' alignment of the crystal's b^* axis with the data-collection spindle axis. $\angle\Omega b^*$ is the inclination of b^* w.r.t. the spindle axis.

Set	$\angle\Omega b^*$	Completeness (%)	Multiplicity	R_{merge}†	R_{meas}‡	R_{meas0}‡
DS1	1.5	88.3	3.9	0.041	0.052	0.071
DS2	41.7	99.4	6.4	0.049	0.057	0.068
Both	1.5 and 41.7	99.4	9.9	0.092	0.102	0.108

† Merging R factor defined as $\sum_{\mathbf{h}}\sum_i |I^i_{\mathbf{h}} - \overline{I}_h|/\sum_{\mathbf{h}}\sum_i I^i_{\mathbf{h}}$. ‡ Multiplicity-weighted R_{merge} (Diederichs & Karplus, 1997). R_{meas} treats anomalous pairs as separate whereas R_{meas0} assumes anomalous pairs to be equivalent.

measurements. This was accompanied by an approximately linear unit-cell dimension increase of 0.3 Å in a and b, and 0.45 Å in c (see Fig. 1), a radiation damage indicator suggested by Ravelli *et al.* (2002). It was also noticed that certain regions of the data had suffered (as indicated by high image R_{merge} values) because of instabilities in either the beam intensity or the beam-intensity monitoring system. This meant that after careful selection of images which had apparently not suffered from this problem, only 108° from DS1 and all 200° from DS2 were worth retaining for further analysis. Table 1 shows the results of integration and scaling for the unaffected data from DS1 and DS2 separately and for both merged together. The scaling was performed using protocols described in the *SCALA* documentation (Collaborative Computational Project, Number 4, 1994) whereby DS1 was first scaled and merged to create a reference data set and DS2 was then scaled to this reference and subsequently merged. Absorption corrections determined in the crystal's frame of reference were applied to DS1 and DS2.

The presence of an anomalous signal in the two data sets was clearly indicated by differences between plots of R_{meas} and R_{meas0} shown in Fig. 2. The quality of both data sets at low resolution was comparable, as seen from the values of R_{meas}. However, a significant decrease in R_{meas0} at low resolution suggested a decrease in the anomalous signal present in DS2 with respect to DS1, possibly as a result of a change to the structure of anomalous scatterers within the crystal.

The DS1 data were input to *SHELXD* (Usón & Sheldrick, 1999), which found 11 heavy-atom positions. These sites were input, together with the DS1 SAD data, into *autoSHARP* (Vonrhein & Bricogne, 2003) which identified seven new heavy-atom sites but, after solvent flattening with *DM* (Cowtan, 1994) and *SOLOMON* (Abrahams & Leslie, 1996), did not produce a map of sufficient quality to allow automatic model building with *ARP/wARP* (Perrakis *et al.*, 1999) (see job i in Table 2). On closer inspection of the electron density in conjunction with a refined model of the elastase molecule, the map did in fact appear to contain detail which resembled protein peptides with clearly visible side-chain density; however, it suffered from very poor connectivity which made interpretation impossible. It seemed very likely that this was owing to the low overall completeness of the DS1 data and the fact that a separate low-exposure pass had not been performed to remeasure strong low-resolution reflections which were missed owing to detector-saturation effects.

The 18 heavy-atom sites were therefore used in *SHARP* with the DS1 and DS2 data together. Given the poor merging statistics between the two data sets and the observed decrease in anomalous signal, suggesting some change to the heavy-atom substructure, the data sets were input as separate crystals into *SHARP*, so that the heavy-atom positions would be common between DS1 and DS2 but their occupancies and B factors would be refined individually along with non-isomorphism parameters. This time, the electron-density map

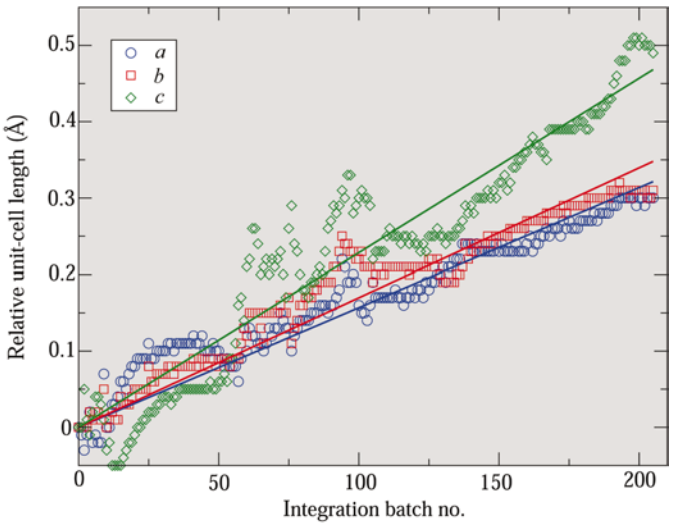

Figure 1
Changes observed in the unit-cell lengths of PPE over the course of 1600 s total exposure to 2.0 Å X-rays. The increase in unit-cell dimensions, and therefore unit-cell volume, is a direct result of radiation damage to the crystal sample.

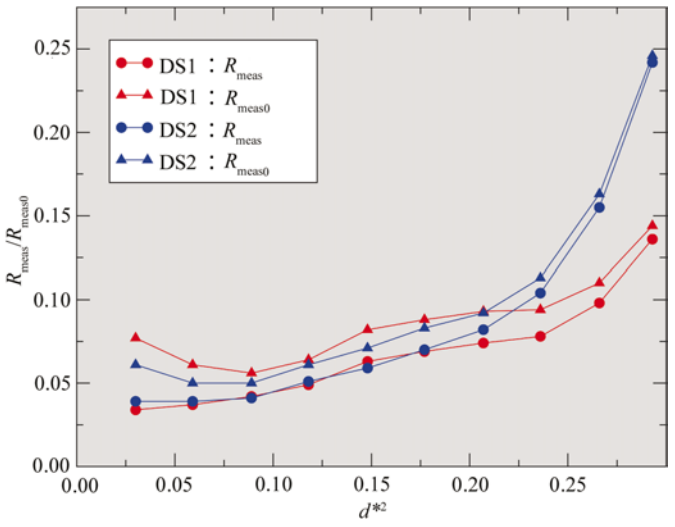

Figure 2
Multiplicity-weighted R factors, R_{meas} and R_{meas0}, plotted as a function of resolution for data sets DS1 and DS2. The difference between values of R_{meas} and R_{meas0} are an indication of the magnitude of the anomalous signal present in the data.

Table 2
Result of phase determination, solvent flattening and automatic model building for I-SAD using (i) DS1 data alone, (iia) DS2 data alone with sites from DS1, (iib) DS2 data alone with sites from DS2, (iii) DS1 and DS2 with radiation-damage effects modelled, (iv) DS1 and DS2 with radiation effects not modelled and (v) DS1 and 30° of DS2 data with radiation damage modelled.

Where two values of PP-acen Ano are specified they refer to data from sets DS1 and DS2, respectively. PP-cen and PP-acen are the overall phasing powers reported by *SHARP* for centric and acentric reflections respectively. PPC and $\Delta\varphi$ are respectively the phased correlation coefficient and the r.m.s. phase difference determined relative to calculated structure factors for the refined atomic model. The results of automatic building are shown as $N/R(PnQd)$ representing N out of a total R peptides built in $P + Q$ chains. P chains were built as polyalanine and Q chains were successfully docked into the amino-acid sequence. The *ARP*/*wARP* results serve as a qualitative indicator of the electron-density map interpretability.

	PP-cen	PP-acen		*SHARP*		*SOLOMON*		*ARP*/*wARP*	
Job	Iso	Iso	Ano	PCC	$\Delta\varphi$ (°)	PCC	$\Delta\varphi$ (°)	No. residues	R.m.s. difference (Å)
(i)	—	—	1.828	0.493	47.4	0.665	38.2	14/240 (3*n*)	1.568
(iia)	—	—	1.417	0.441	50.3	0.642	38.8	215/240 (2*n*4*d*)	0.179
(iib)	—	—	1.305	0.427	51.0	0.612	41.3	217/240(3n4d)	0.210
(iii)	0.405	0.423	2.184/1.531	0.549	44.5	0.821	24.8	230/240 (2*n*2*d*)	0.163
(iv)	—	—	1.843/1.711	0.478	49.3	0.736	31.9	230/240 (4*d*)	0.157
(v)	0.336	0.334	2.029/1.796	0.522	45.7	0.757	30.4	225/240 (5*d*)	0.169

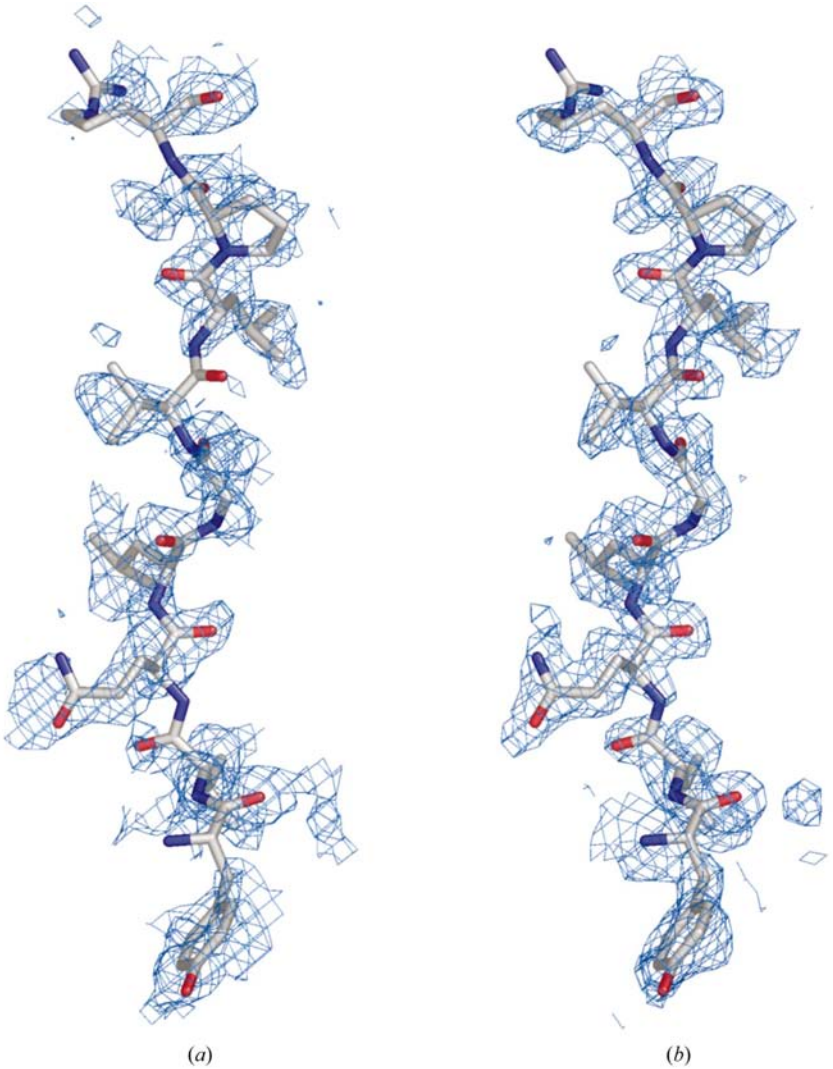

Figure 3
Electron-density maps after solvent flattening with *SOLOMON* around part of the refined PPE model from Tyr117 to Arg125. (*a*) shows the map from job i using DS1 data. The map is poorly connected and contains four breaks along the main chain. (*b*) shows the same region after inclusion of DS1 and DS2 data (job iii). The connectivity is improved leaving only one break along the main chain.

produced by *SHARP* and *SOLOMON* allowed *ARP*/*wARP* to build 230 out of 240 residues in four peptide chains, two of which were successfully docked into the amino-acid sequence (see job iii in Table 2). Fig. 3 shows the improvement in electron density obtained by including the DS2 data in the phase determination.

The isomorphous phasing power between DS1 and DS2 of 0.405 for centric and 0.423 for acentric reflections indicated that a significant phasing signal was indeed being generated by this treatment of radiation damage. This was supported by the consistent decrease observed in the refined occupancies of all heavy atoms in set DS2 with respect to DS1 (see Fig. 4), and this was further tested by running *SHARP* for the DS1 and DS2 data under the assumption that the heavy-atom model was the same for both. This control run was performed by including the data as separate batches of the same crystal within *SHARP* (See job iv in Table 2). Fig. 5 shows the beneficial effects of modelling the radiation damage in the heavy-atom model, in the form of improved phased correlation coefficients[3] (PCCs) calculated relative to refined model amplitudes and phases in both the experimental maps and solvent-flattened maps. The observed increase in PCC varies from between 0.2 at low resolution to 0.05 at 1.85 Å.

Interestingly, the isomorphous-difference residual maps calculated by *SHARP* after job (iii) showed evidence of additional radiation damage in the form of negative peaks of

[3] The phased correlation coefficient (PCC) is equivalent to the map correlation coefficient, but calculated in reciprocal space by Parseval's theorem and binned as a function of resolution (Bricogne, 2003).

between -4.3σ and -7.8σ in height located at the S atom positions of the Cys58–Cys42 and Cys168–Cys183 disulfide bridges. Such effects were reported by Ravelli & McSweeney (2000) in their studies of radiation damage. Inclusion of these sulfur positions into the heavy-atom model produced no significant improvement in the resulting phases, however, because the majority of the phasing signal was already being generated by the strong iodine anomalous signal and the iodine occupancy changes.

To verify that incompleteness of the DS1 data was the probable cause of the poor map quality from job (i), 30° of the DS2 data (sufficient to achieve 97.4% overall completeness and a multiplicity of 4.6) were used with the DS1 data in *SHARP*. The results (job v in Table 2) confirm that an interpretable map can be obtained from low-redundancy I-SAD data collected at long wavelengths. In fact using the 18 sites determined from job (i) with the data from DS2 only in *SHARP* also produced an interpretable map (see job iia in Table 2). However, it would not be advisable to set out to routinely obtain phases in this manner. The DS2 data alone was in fact sufficient for structure solution, but *SHELXD* and *autoSHARP* could find only 12 sites for use in the phase determination. The results (job iib in Table 2) are comparable but slightly worse than those for job (iia). The difference in the number of sites detected using DS2 compared with DS1 is most probably an indication of the disruption of the heavy-atom substructure with time and/or the inherently higher accuracy of the anomalous differences recorded for DS1.

An experiment about a single axis is certainly the easiest to perform and offsetting the crystal to obtain complete data is advisable and indeed routine. However, in low-symmetry space groups this may improve ordinary completeness (w.r.t. unique indices under Laue symmetry) but fail to improve anomalous completeness to the same extent. In such cases, the use of two orientations would be a much more effective strategy for obtaining a complete set of anomalous differences with balanced multiplicities.

4. Discussion

We have used elastase, which is unusually stable, but the triiodide-soak method has also proved applicable to other proteins (Evans & Bricogne, 2002). A recent example of its use on the γ-adaptin appendage domain (Evans & Bricogne, 2003) shows that it is applicable to proteins involved in 'real' structural biology problems. Even using this robust sample, however, we have observed significant radiation damage effects arising from the presence of I atoms in the crystal which resulted in poor merging of measurements from that crystal

What is clearly demonstrated here is the 'site-specific' nature of radiation damage in the case of iodine, so much so that inclusion of the radiation-modified heavy-atom model into phase determination produced an extra 'isomorphous' phasing power of over 0.4, resulting in an average improvement in the phased correlation coefficients of about 0.1. For borderline cases this improvement would be significant in terms of electron-density interpretation.

Recently, it has in fact been shown that specific radiation damage can be used as the sole source of phase information in the solution of some macromolecular structures (Ravelli *et al.*, 2003).

One might expect the sensitivity of I atoms to radiation to vary according to chemical environment or bonding. Such a correlation was not observed in this case, but a more

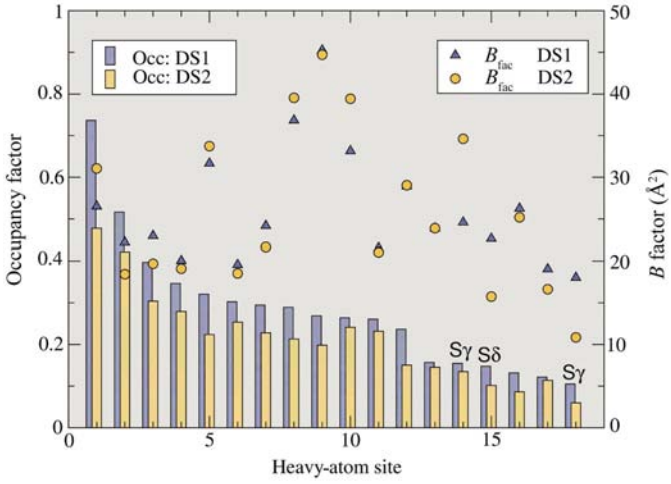

Figure 4
Occupancy and *B* factors refined by *SHARP* for data sets DS1 and DS2 in job (iii). A total of 18 heavy atoms were refined as I atoms although it was later noticed that three of the sites were in fact S atoms from two cysteines of a disulfide bridge and a methionine. There is a relative decrease in the occupancy factors for all heavy atoms of between 7 and 37% for DS2 data compared with their values for DS1 data, whereas the *B* factor of all the I atoms changes by on average 2.1 Å^2. The S atom *B* factors on the other hand differ significantly between DS1 and DS2.

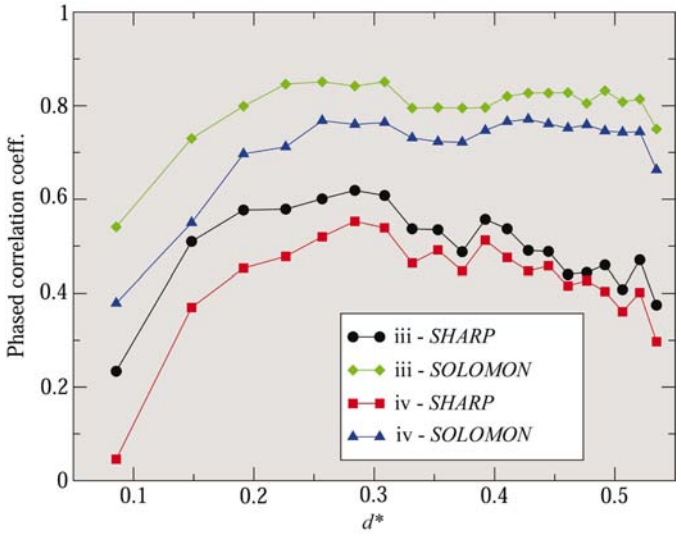

Figure 5
Phased correlation coefficients as a function of resolution for phases produced by *SHARP* and phases after solvent flattening with *SOLOMON*. In both cases shown, data sets DS1 and DS2 were included into the *SHARP* jobs with 18 heavy-atom sites. However, in one case (iv) the heavy-atom model was common to both data sets whereas in the other (iii) different occupancies and *B* factors were refined for DS1 and DS2 so that advantage could be taken of heavy-atom-specific radiation-damage effects.

systematic study would be necessary before drawing any conclusions about the existence or otherwise of such effects.

In retrospect, the experimental protocol used to record these data was far from optimal. The initial intention of recording data in two orientations from the same sample, to allow a better correction of absorption effects, was mostly defeated owing to the unanticipated severity of radiation-damage effects. This made it impossible to adequately merge the data from the two orientations together because they were no longer the same sample. The handling of absorption effects, however, did not turn out to play a significant role in structure determination. The anomalous signal-to-noise ratio produced by the triiodide derivative at a wavelength of 2.0 Å was sufficient to allow heavy-atom substructure determination from data recorded with an average multiplicity of 3.9, *i.e.* on average only two measurements of each equivalent Bijvoet mate. Map interpretation from the resulting phases was, however, limited only by incompleteness of the data from the first orientation, a direct result of the initial data-collection strategy adopted and the reason why the inclusion of data from the second orientation was essential. An interpretable map was later obtained by the addition of only 30° of data from that second orientation.

Also highlighted here is the importance of data-collection strategies which not only aim to record a complete set of data by the end of the experiment, but aim to record as much essential data as soon as possible in the experiment in case radiation effects become appreciable. In our case, recording data in multiple orientations should have been performed by regular adjustment of the crystal orientation in such a way that it allowed effective sampling of the absorption surface as well as the fastest accumulation of a complete data set. Such strategies are currently being developed by the authors.

The alignment of the crystal in DS1 allowed the measurement of accurate anomalous differences for use in heavy-atom detection by *SHELXD* and these data did not benefit greatly from absorption corrections. This was reflected in the very small refined values of spherical harmonic coefficients (SHCs) in *SCALA*. However, a negative consequence of the alignment was that the DS1 data suffered from incompleteness. This in turn could only be overcome by making measurements with the sample misaligned, thereby recreating the need for effective absorption corrections as indicated by significantly larger refined values of the SHCs for DS2 compared with DS1.

5. Conclusions

We have demonstrated that low-redundancy data recorded using softer X-rays (λ = 2.0 Å) can be used successfully with a short-soak triiodide derivatization to generate SAD phases of sufficient quality to allow structure determination in a nearly automatic 'high-throughput' fashion.

Furthermore, radiation damage, manifested as a reduction in iodine occupancy factors, can be exploited straightforwardly in *SHARP* to generate additional phase information and improve the final electron-density map. This is accomplished through the very simple device of declaring different time batches of data as distinct crystals of the same compound, rather than as distinct data batches for a unique crystal and wavelength.

The authors would like to thank Dr Clemens Vonrhein for his invaluable assistance with the use of *autoSHARP*. We are also grateful to Drs J. Pflugrath and J. Ferrara for access to the latest versions of *d*TREK*. This work was partly supported by a European Commission grant No. HPRI-CT-1999-50015 within the EXMAD project.

References

Abrahams, J. P. & Leslie, A. G. W. (1996). *Acta Cryst.* D**52**, 30–42.
Arndt, U. W. (1984). *J. Appl. Cryst.* **17**, 118–119.
Bricogne, G. (2003). To be published.
Cianci, M., Rizkallah, P., Olczak, A., Raftery, J., Chayen, N. E., Zagalsky, P. F. & Helliwell, J. R. (2001). *Acta Cryst.* D**57**, 1219–1229.
Collaborative Computational Project, Number 4 (1994). *Acta Cryst.* D**50**, 760–763.
Cowtan, K. (1994). *Jnt CCP4/ESF–EACBM Newsl. Protein Crystallogr.* **31**, 34–38.
Cromer, D. T. & Liberman, D. (1970). *J. Chem. Phys.* **53**, 1891–1898.
Dauter, Z. (2002). *Curr. Opin. Struct. Biol.* **12**, 674–678.
Dauter, Z., Dauter, M. & Rajashankar, K. (2000). *Acta Cryst.* D**56**, 232–237.
Diederichs, K. & Karplus, P. A. (1997). *Nature Struct. Biol.* **4**, 269–275.
Djinovic Carugo, K., Everitt, P. & Tucker, P. A. (1998). *J. Appl. Cryst.* **31**, 812–814.
Evans, G. & Bricogne, G. (2002). *Acta Cryst.* D**58**, 976–991.
Evans, G. & Bricogne, G. (2003). In the press.
Evans, P. R. (1997). *Proceedings of the CCP4 Study Weekend. Recent Advances in Phasing*, edited by K. S. Wilson, G. Davies, A. W. Ashton and S. Bailey. Warrington: Daresbury Laboratory.
Konishi, T., Tanaka, W., Kawai, T. & Fujikawa, T. (2001). *J. Synchrotron Rad.* **8**, 737–739.
Micossi, E., Hunter, W. N. & Leonard, G. A. (2002). *Acta Cryst.* D**58**, 21–28.
Nagem, R. A. P., Dauter, Z. & Polikarpov, I. (2001). *Acta Cryst.* D**57**, 996–1002.
Panjikar, S. & Tucker, P. A. (2002*a*). *J. Appl. Cryst.* **35**, 261–266.
Panjikar, S. & Tucker, P. A. (2002*b*). *Acta Cryst.* D**58**, 1413–1420.
Perrakis, A., Morris, R. J. & Lamzin, V. S. (1999). *Nature Struct. Biol.* **6**, 458–463.
Pflugrath, J. W. (1999). *Acta Cryst.* D**55**, 1718–1725.
Polentarutti, M. & Djinovic Carugo, K. (2003). In preparation.
Ravelli, R. B. G., Leiros, H.-K. S., Pan, B., Caffrey, M. & McSweeney, S. (2003). *Structure*, **11**, 217–224.
Ravelli, R. B. G. & McSweeney, S. M. (2000). *Structure*, **8**, 315–328.
Ravelli, R. B. G., Theveneau, P., McSweeney, S. & Caffrey, M. (2002). *J. Synchrotron Rad.* **9**, 355–360.
Sauer, O., Schmidt, A. & Kratky, C. (1997). *J. Appl. Cryst*, **30**, 476–486.
Sun, P. D. & Radaev, S. (2002). *Acta Cryst.* D**58**, 1099–1103.
Sun, P. D., Radaev, S. & Kattah, M. (2002). *Acta Cryst.* D**58**, 1092–1098.
Usón, I. & Sheldrick, G. (1999). *Curr. Opin. Struct. Biol.* **9**, 643–648.
Vonrhein, C. & Bricogne, G. (2003). To be published.
Weiss, M. S., Sicker, T., Djinovic Carugo, K. & Hilgenfeld, R. (2001). *Acta Cryst.* D**57**, 689–695.